IEEE Access
Multidisciplinary ⋮ Rapid Review ⋮ Open Access Journal

Received 24 December 2023, accepted 1 January 2024, date of publication 9 January 2024,
date of current version 19 January 2024.

Digital Object Identifier 10.1109/ACCESS.2024.3351675

RESEARCH ARTICLE

Optimizing CZTSe Solar Cell Architecture: Comparative Study of ZnO, TiO_2, and MoO_3 as Electron Transport Layers

JASURBEK GULOMOV[1], OUSSAMA ACCOUCHE[2], (Member, IEEE), JAKHONGIR ZIYOITDINOV[3], AND AVAZBEK MIRZAALIMOV[3]

[1]Andijan State Pedagogical Institute, Andijan 170100, Uzbekistan
[2]College of Engineering and Technology, American University of the Middle East, Egaila 54200, Kuwait
[3]Department of General Physics, Andijan State University, Andijan 170100, Uzbekistan

Corresponding author: Jasurbek Gulomov (jasurbekgulomov@yahoo.com)

ABSTRACT This study investigates the optimization of $Cu_2ZnSnSe_4$(CZTSe)-based solar cells by employing distinct charge transport layers (CTLs) for enhancing their efficiency. ZnO, TiO_2, and MoO_3 are evaluated as electron transport layers (ETLs), while NiOx serves as a hole transport layer (HTL). By systematically varying ETL and CZTSe layer thicknesses, the influence of these parameters on solar cell performance is explored. According to obtained results, it has been found that the optimum size of base and emitter layers are equal to 2 μm and 80 nm in n-ZnO/p-CZTSe/p-NiO_x, 1.5 μm and 60 nm in n-TiO_2/p-CZTSe/p-NiO_x, as well as 1 μm and 60 nm in n-MoO_3/p-CZTSe/p-NiO_x. Maximum efficiencies of n-ZnO/p-CZTSe/p-NiO_x, n-TiO_2/p-CZTSe/p-NiO_x, and n-MoO_3/p-CZTSe/p-NiO_x solar cells with optimal sizes are equal to 21.35%, 21.76% and 24.14%, respectively. So, MoO_3 with thickness of 60 nm is the optimal ETL for CZTSe based solar cell due to forming high electric field and large electrostatic potential difference which helps to separate effectively the photogenerated electron-hole pairs. Each solar cells reached to maximum open circuit voltage at minimum base thickness and to maximum short circuit current at maximum base thickness. Furthermore, the study assesses the potential of CZTSe, a promising alternative to traditional silicon-based solar cells, as it exhibits a tunable bandgap allowing for efficient sunlight absorption. The investigation delves into the unique ETL/CZTSe/HTL structure, utilizing ZnO, TiO_2, and MoO_3 as ETLs and NiOx as the HTL. The results reveal that MoO_3, with a thickness of 60 nm, emerges as the optimal ETL for CZTSe-based solar cells, achieving a peak efficiency of 24.14% due to its ability to create a high electric field and significant electrostatic potential difference, enhancing the effective separation of photogenerated electron-hole pairs. Additionally, the study explores the interplay between emitter and base layer thicknesses, demonstrating the impact on open circuit voltage and short circuit current, providing valuable insights for the design and optimization of CZTSe-based solar cells.

INDEX TERMS Numerical simulation, heterojunctions, zinc oxide, titanium dioxide.

I. INTRODUCTION

Today, solar cells are considered as one of the most effective means of covering the need for energy. Increasing the efficiency of solar cells and reducing their cost is one of the important tasks. 90% of industrial solar cells are made of silicon [1]. According to the theory, the efficiency of silicon-based solar cells does not exceed 29% [2]. To overcome this theoretical limit, the formation of tandem structures [3] and nanoparticle [4] or quantum dot [5] insertion methods are proposed. When platinum nanoparticles are introduced into a silicon-based solar cell, the efficiency is found to increase by up to 2 times [6]. By creating a tandem structure or introducing nanoparticles, the efficiency of silicon-based solar cells can be increased, but the cost cannot be reduced, on the contrary, it increases. Therefore,

The associate editor coordinating the review of this manuscript and approving it for publication was Guido Lombardi.

new materials are being tested to replace silicon to create high-efficiency and low-cost solar cells. For example, today materials such as perovskite [7] and kasterite [8] are easy to synthesize and inexpensive, so interest in photovoltaics has increased dramatically. Perovskite-based solar cells have high efficiency, but low stability and toxicity [9]. The stability is high and the non-toxic ones have a low efficiency. The tunable bandgap of kasterite allows for efficient absorption of a broader spectrum of sunlight, making it more suitable for capturing solar energy compared to silicon, which has a fixed bandgap. The synthesis of kasterite, a promising alternative to silicon in solar cell applications, typically involves methods such as sputtering, chemical bath deposition, or other thin film deposition techniques. In contrast to the complex and energy-intensive processes associated with silicon fabrication, kasterite synthesis offers a more environmentally sustainable approach, leveraging earth-abundant elements for efficient and cost-effective solar cell production. Kasterite-based solar cells are highly stable and non-toxic, but so far have a low efficiency in experiments.

The most common kasterite materials used in photovoltaics are Cu_2ZnSnS_4 (CZTS) [10] and $Cu_2ZnSnSe_4$ [11]. By controlling the mixed selenium and sulfur atoms and their ratio, the band gap of CZTSSe can be changed from 1 eV to 1.5 eV [12]. The band gap of CZTSe is 1 eV and that of CZTS is 1.5 eV. The maximum efficiency of the CZTSe-based solar cell is equal to 10.54% in experiment [13] and 18.63% in modeling [14]. The efficiency of CZTS-based solar cell is 12.5% in experiment [15] and 25.3% in modeling [16]. In the experiment, by controlling the atomic ratios of S/(S+Se), Cu/(Zn+Sn) and Zn/Sn, the concentration of deleterious defects (N_t>1e16) in CZTSSe was reduced and a maximum efficiency of 19.06% was achieved [17]. The optimal value of the S/S+Se ratio in CZTSSe was found to be 0.4 [18]. In addition, since CZTS and CZTSe have different band gaps, tandem solar cells are designed based on them. A CZTS/CZTSe tandem solar cell with an efficiency of 26.21% was designed in simulation [19].

CZTS and CZTSe materials have p-type conductivity due to copper vacancy [20]. In CZTSe-based solar cells, mainly contact/WindowLayer/BufferLayer/CZTSe/Contact structure solar cells have been studied. Materials such as ZnO and CdS or ZnSe were used as the window layer and as the buffer layer. However, their efficiency in simulation is also low. CZTSe structures in other architectures should be investigated. Therefore, in this scientific work, we researched the ETL/CZTSe/HTL structure, which is different from the previous structures. ZnO, TiO_2 and MoO_3 were selected as ETL and NiO_x as HTL. Because metal oxide can act as an anti-reflection layer and a transparent contact at the same time. Besides, fabrication of metal oxides using sol-gel method is easy. Metal oxides like ZnO, TiO_2 and MoO_3 form naturally n type conduction and NiO_x form p type conduction because of vacancies. CZTSe has a large absorption coefficient in thin films. Also, the influence of the ETL layer solar cell on the optical and electrical parameters is significant. Therefore, in this paper, the optimal metal oxide for ETL and the optimal thicknesses of CZTSe and ELT is determined. By investigating the unique ETL/CZTSe/HTL structure with ZnO, TiO_2, MoO_3, and NiO_x, this research pioneers an innovative approach in CZTSe-based solar cell design. The strategic use of metal oxides as ETL and HTL materials not only simplifies fabrication with the sol-gel method but also promises enhanced optical and electrical parameters, underscoring the potential for breakthroughs in efficient and cost-effective photovoltaic technologies.

The article consists of 4 parts: Introduction, material and method, result and discussion, and conclusion.

II. MATERIALS AND METHODS

In there are 3 main methods of studying solar cells: theory, experiment, and simulation. In this scientific work, CZTSe based solar cells with charge transport layers were investigated by simulation in Sentaurus TCAD. Four main tools of Sentaurus TCAD were used for simulation: Sentaurus Structure Editor, Sentaurus Device, Sentaurus Workbench and Sentaurus Visual. A geometric model of the solar cell was created in the Sentaurus Structure Editor. In CZTSe based solar cell, ZnO, TiO_2 and MoO_3 as ETL and NiO_x as HTL are used.

After the geometric model is developed, the properties of the necessary materials are given in Sentaurus Device. Table 1 shows the physical parameters of materials in the studied solar cell required for simulation. In device simulation, the geometric model and physical parameters of the desired material are used as input parameters.

TABLE 1. Physical parameters of CZTSe [22], [23], NiO_x [24], TiO_2 [25], ZnO [26], [27], [28] and MoO_3 [29], [30].

Properties	CZTSe	ZnO	TiO_2	MoO_3	NiO_x
E_g, eV	1	3.3	3.2	3.03	3.8
E_{aff}, eV	4.35	4.5	4.2	6.6	1.6
ε	13.6	8.5	12.3	58	11
N_c, cm^{-3}	2.2×10^{18}	2.2×10^{18}	2×10^{17}	2.45×10^{15}	1×10^{18}
N_v, cm^{-3}	1.8×10^{19}	1.8×10^{19}	6×10^{17}	4.55×10^{15}	1×10^{18}
m_e	0.07	0.24	0.5	0.61	1
m_h	0.2	0.59	4.66	1.13	0.8
μ_e, $cm^2V^{-1}s^{-1}$	145	50	18.6	3811	2.8
μ_h, $cm^2V^{-1}s^{-1}$	35	5	3.1	1609	2.8

The width of the solar cell was 10 μm, and the HTL layer thickness was 100 nm. The ETL layer thickness was changed from 20 nm to 200 nm and the CZTSe layer thickness was changed from 0.5 μm to 5 μm. In Sentaurus Structure Editor, addition to geometric model, material type, input concentration and mesh sizes are also given. 1×10^{17} cm^{-3} of donor, 1×10^{15} cm^{-3} and 1×10^{16} cm^{-3} of acceptor were doped to ETL, base and HTL layers, respectively. The size of the mesh was changed depending on the thickness of the base and emitter layers. Due to the presence of active and passive regions in the solar cell [21], it is meshed with 2 different sizes. The

general area is meshed larger and the active areas smaller. The dimensions of the mesh in the general area of the solar cell were taken equal to 1/500 of the base thickness on the Y axis and 1/500 of the width on the X axis. In heterojunctions such as ETL/CZTSe and CZTSe/HTL, the mesh sizes of the active areas were taken equal to 1/200 of the emitter thickness on the Y axis and 1/1000 of the width on the X axis. Sentaurus Visual is used to visualize the geometric model and display the obtained results graphically. Sentaurus Workbench is an environment that provides integration of all tools. In addition, it is possible to recalculate the model by giving values to the variables created during the creation of a geometric model.

The light spectrum is also important in simulation of the solar cell. In this study, CZTSe-based solar cells were illuminated with AM1.5G spectrum. Besides, light is incident to structures normal to their surface. After providing the necessary input parameters, the calculation is performed on the Sentaurus Device. Firstly, the optical properties of the solar cell are determined. The optical properties of planar CZTSe-based solar cells were calculated using the Transfer Matrix Method (TMM) [31]. Because TMM is mainly designed for the calculation of planar optical systems, its advantage also takes into account internal interference in thin layers. In reality, there is no such thing as an absolutely smooth surface. There are also small reliefs on the surface of the planar solar cell. In order to take into account light scattering from surface reliefs, it is necessary to modify the matrix elements of TMM using haze parameters given formula 1. The ratio of the light scattered from the surface to the total light incident on the surface is called the haze parameter.

$$
\begin{aligned}
&H^{r}_{j,j+1}\left(\lambda,\varphi_j\right)\\
&=1-\exp\left[-\left(\frac{4\pi\sigma_{rms}c_r\left(\lambda,\sigma_{rms}\right)n_j\cos\varphi}{\lambda}\right)^{a^r}\right]\\
&H^{t}_{j,j+1}\left(\lambda,\varphi_j\right)\\
&=1-\exp\\
&\times\left[-\left(\frac{4\pi\sigma_{rms}c_t\left(\lambda,\sigma_{rms}\right)\left|n_j\cos\varphi_j-n_{j+1}\cos\varphi_{j+1}\right|}{\lambda}\right)^{a^t}\right]
\end{aligned}
\tag{1}
$$

Here: σ_{rms} is mean square roughness of the surface, $a^{r/t}$ and $c_{r/t}$ *are* fixing parameters, n is refractive index, λ is wavelength, φ is angle of scattering.

The theory of scalar scattering [32] calculates the scattering of light from surface. Light is scattered from a textured surface at different angles, and the scattering is calculated by an angle-dependent angular distribution function [33]. Haze parameters are calculated to modify the reflection and transmission parameters. The Haze function adapts the elements of the matrix designed to calculate the transmission and reflection coefficients in the TMM to take into account the scattered light.

At the boundary between two media, light refracts and reflects. They are calculated using optical boundary conditions. There are two types of optical boundary conditions: angle and energy. The angle distribution between the refracted and reflected light is calculated by Snell's law and the energy distribution is calculated by the Fresnel coefficients given in formula 2 [34].

$$
\begin{cases} r_t=\dfrac{n_1\cos\beta-n_2\cos\gamma}{n_1\cos\beta+n_2\cos\gamma}\\ t_t=\dfrac{2n_1\cos\beta}{n_1\cos\beta+n_2\cos\gamma}\end{cases}
\quad and \quad
\begin{cases} r_p=\dfrac{n_1\cos\gamma-n_2\cos\beta}{n_1\cos\gamma+n_2\cos\beta}\\ t_p=\dfrac{2n_1\cos\beta}{n_2\cos\beta+n_1\cos\gamma}\end{cases}
\tag{2}
$$

Here*:* r_t and t_t are the Fresnel coefficients for transversal polarized light, r_p and t_p are the Fresnel coefficients for parallel polarized light, β is the angle of incident light, γ is the angle of refracted light.

After determining the optical properties, the amount of photogeneration is calculated by the quantum yield function. If the energy of the photon is greater than the bandgap of the material, the quantum yield is equal to 1 and an electron-hole pair is formed, otherwise it is equal to zero and no electron is generated. Electrons and ions create an electric field. The electric field and electric potential at each node of the mesh are calculated by the Poisson equation given in formula 3 [35].

$$
\Delta\varphi=-\frac{q}{\varepsilon}\left(p-n+N_D+N_A\right)
\tag{3}
$$

Here: ε is the permittivity, N_D and N_A are the concentrations of donor and acceptor, q is the charge.

Since electrons belong to the fermions, their concentration is calculated by the Fermi function [36] given in formula 4. In simulation, the concentration of electrons in a semiconductor is determined by calculating the Fermi function in a numerical method or the Boltzmann approximation in an analytical method. In this paper, the Fermi function was calculated numerically. Because the error of the Boltzmann approximation increases as the input concentration increases. By calculating the Fermi function, the value of p and n in the Poisson equation, which is the concentration of electrons and holes in the mesh nodes, is determined.

$$
\begin{aligned}
n&=N_cF_{1/2}\left(\frac{E_{F,n}-E_c}{kT}\right)\\
p&=N_VF_{1/2}\left(\frac{E_V-E_{F,p}}{kT}\right)
\end{aligned}
\tag{4}
$$

Here: N_c and N_v are the densities of the states in the conduction and the valence bands, respectively, E_c is the minimum energy of the conduction band, E_v is the maximum energy of the valence band, T is the temperature, k is the Boltzmann constant, and $E_{F,n}$ and $E_{F,p}$ are the quasi-fermi energies.

Charge carriers move due to internal electric field and concentration difference. The most common physical model for calculating the transport of charge carriers is the Drift-Diffusion model. This article also used the Drift-Diffusion model [37] given in formula 5. Because the effect of temperature on the properties of CZTSe solar cell has not been studied. The drift-diffusion model can only calculate the charge carriers transport in a solar cell at a temperature of 300 K.

$$J_n = -nq\mu_n \nabla \Phi_n$$
$$J_p = -pq\mu_p \nabla \Phi_p \tag{5}$$

Here: μ_n, μ_p are the mobilities of electron and holes, F_n, F_p are the electron and hole quasi-Fermi potentials, P_n, P_p are the thermoelectric power of electrons and holes, T is the absolute temperature.

Charge carriers recombine when they move. There are 3 main types of recombination in semiconductors: radiative, Shockley Read Hall (SRH) and Auger. ZnO [38], TiO_2 [39] and NiO_x [40] being a direct semiconductor, they also have triplet recombination. CZTSe and MoO_3 [41] are indirect semiconductors so they mainly have SRH and Auger recombination. Amount of radiative recombination is less than 1%, so it is not necessary to calculate radiative recombination in these semiconductors in simulation. Ohmic contacts are used to prevent overheating and reduce charge carrier loss. The potential generated in the contacts are determined by the Ohmic boundary conditions given in formula 6.

$$\varphi = \varphi_F + \frac{kT}{q} \operatorname{asinh}\left(\frac{N_D - N_A}{2n_{i,eff}}\right)$$
$$n_0 p_0 = n_{i,eff}^2$$
$$n_0 = \sqrt{\frac{(N_D - N_A)^2}{4} + n_{i,eff}^2} + \frac{N_D - N_A}{2}$$
$$p_0 = \sqrt{\frac{(N_D - N_A)^2}{4} + n_{i,eff}^2} - \frac{N_D - N_A}{2} \tag{6}$$

Here: $n_{i,eff}$ is concentration of effective intrinsic carrier, φ_F is Fermi potential of contact.

III. RESULTS AND DISCUSSION

A. GEOMETRIC STRUCTURE OF CZTSe SOLAR CELLS

CZTSe is a good light-absorber. Charge transport layers are used to transport the generated electrons and holes to the contacts. In this work, ZnO, TiO_2 and MoO_3 were used as an ETL and NiO_x as HTL. Figure 1 shows the geometric structure of Contact/ETL/CZTSe/HTL/Contact structure and band diagram of CZTSe-based structures with metal oxide charge transport layer. The band offsets between ZnO/CZTSe, TiO_2/CZTSe, MoO_3/CZTSe and CZTSe/NiO_x heterojunctions are 0.15 eV, −0.15 eV, 2.25 eV and 2.75 eV, respectively. According to the values of electronic affinities of materials and band-offsets of heterojunctions, it was found

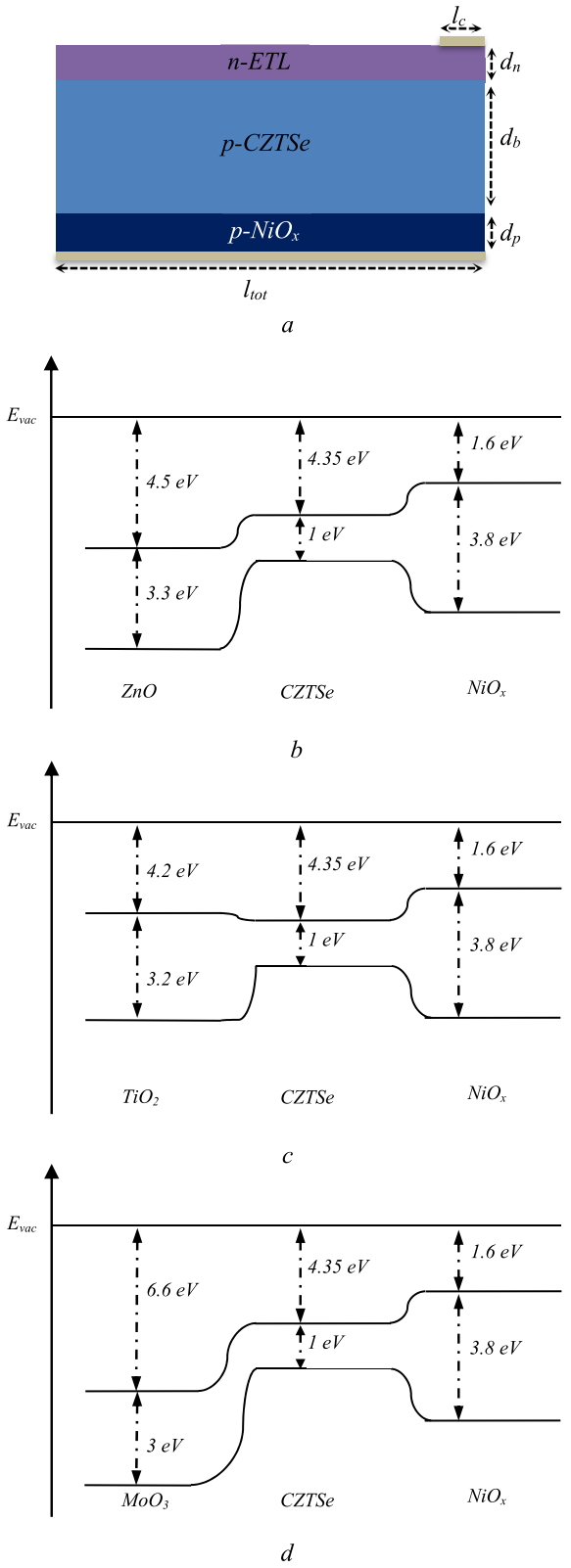

FIGURE 1. Geomtric structure of the CZTSe solar cell (a) and band diagrams of n-ZnO/p-CZTSe/p-NiO_x (b), n-TiO_2/p-CZTSe/p-NiO_x (c) and n-MoO_3/p-CZTSe/p-NiO_x (d) solar cells: l_c and l_{tot} is front contact and total length, d_n, d_b and d_p are thicknesses of ETL, base and HTL layers, respectively.

that electrons move from NiO_x to CZTSe layer and from CZTSe to TiO_2, ZnO or MoO_3 layer.

Holes move in the opposite direction to electrons. This proves that we have chosen the right materials for ETL and HTL. An optimal value of the band-offset [42] also helps to separate the electron-hole pairs generated in the heterojunction and reduce the surface recombination. Efficient separation of charge carriers and their accumulation at the contacts contributes to the improvement of the output power of the solar cell.

B. OUTPUT POWER

Figure 2 shows the dependence of output power of n-ZnO/p-CZTSe/p-NiO_x, n-TiO_2/p-CZTSe/p-NiO_x and n-MoO_3/p-CZTSe/p-NiO_x solar cells on thicknesses of base and ETL layers. The emitter layer thickness was changed from 20 nm to 200 nm. It was found that the maximum output power can be reached when the thickness of the ZnO layer is 80 nm in the n-ZnO/p-CZTSe/p-NiO_x (Fig. 2.a) solar cell. n-TiO_2/p-CZTSe/p-NiO_x (Fig. 2.b) and n-MoO_3/p-CZTSe/p-NiO_x (Fig. 2.c) solar cells reach maximum power when TiO_2 and MoO_3 layer thickness is 60 nm. In the literature [43], the optimal thickness of ZnO in a CZTSSe/ZnO solar cell was experimentally determined to be 100 nm. When 10 nm thick MoO_3 is placed between the back contact and the light absorbing layer for the purpose of band alignment in CZTSe solar cell, it was found that the efficiency increases to 7.1% [44]. It was found to be 23.13% when TiO_2 with thickness of 50 nm was used as ETL in a CZTSe based solar cell [23]. In this work, the efficiency of the n-TiO_2/p-CZTSe/p-NiO_x structure with a TiO_2 layer thickness of 50 nm was equal to 20.9%.

The optimal thickness of the emitter layer for different solar cells was determined using Figure 2. Figure 3 shows the dependence of output power of n-ZnO/p-CZTSe/p-NiO_x, n-TiO_2/p-CZTSe/p-NiOx and n-MoO_3/p-CZTSe/p-NiO_x solar cells with optimal emitter layer thickness on base thickness.

It was found that almost each solar cell has an extremum in the dependence of the output power on the thickness of CZTSe. The n-ZnO/p-CZTSe/p-NiO_x solar cell achieved a maximum power of 13.59 mW/cm2 at a thickness of 2 μm of CZTSe. n-TiO_2/p-CZTSe/p-NiOx and n-MoO_3/p-CZTSe/p-NiO_x solar cells achieved maximum output power of 13.78 mW/cm2 and 15.28 mW/cm2 when the thickness of CZTSe was 1.5 μm and 1 μm.

Considering that the AM1.5G spectrum was used in the simulation, maximum efficiency of n-ZnO/p-CZTSe/p-NiO_x, n-TiO_2/p-CZTSe/p-NiO_x and n-MoO_3/p-CZTSe/p-NiO_x solar cells with optimal emitter and base thickness are equal to 21.35%, 21.76% and 24.14%, respectively.

The maximum output power was observed in MoO_3 and the smallest output power was observed in ZnO emitter layer solar cell. The reason for this is that the band gap of ZnO, TiO_2 and MoO_3 is equal to 3.3 eV, 3.2 eV and 3 eV. Because CZTSe has a bandgap of 1 eV, it can mainly absorb photons larger than 1 eV. Metal oxides used in the emitter layer can also absorb photons larger than its band gap.

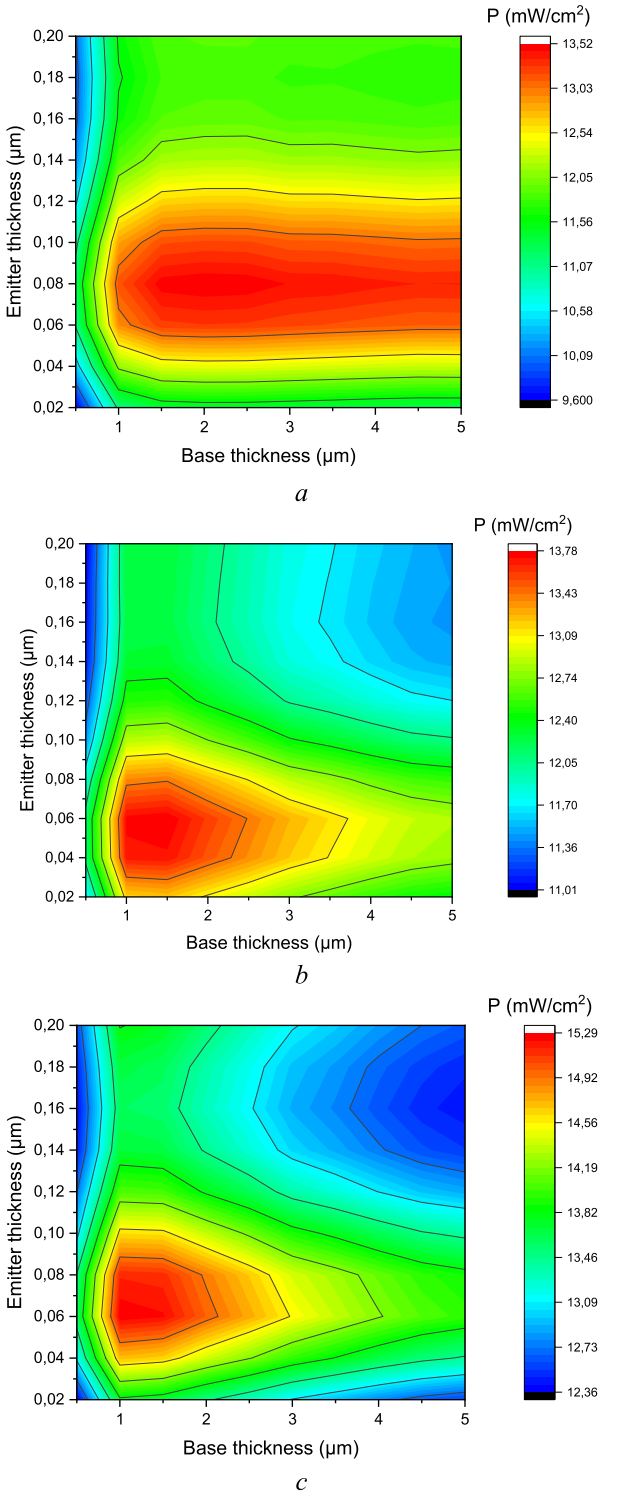

FIGURE 2. Dependence of the output power of n-ZnO/p-CZTSe/p-NiO_x (a), n-TiO_2/p-CZTSe/p-NiO_x (b) va n-MoO_3/p-CZTSe/p-NiO_x (c) on thickness of ETL and base layers.

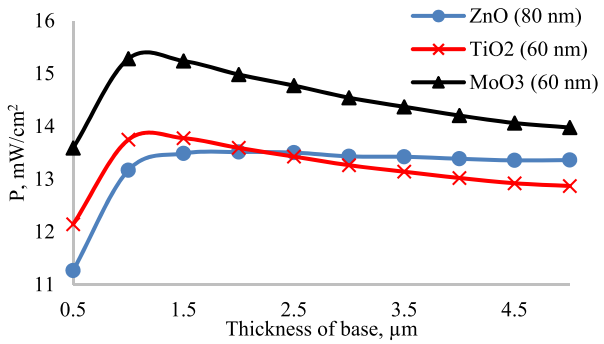

FIGURE 3. Dependence of output power of n-ZnO/p-CZTSe/p-NiO_x solar cell with ETL layer thickness of 80 nm as well as va n-TiO_2/p-CZTSe/p-NiO_x, n-MoO_3/p-CZTSe/p-NiO_x solar cells with ETL layer thickness of 60 nm on thickness of CZTSe layer.

C. SHORT CIRCUIT CURRENT

In the n-ZnO/p-CZTSe/p-NiO_x solar cell, photons with energy greater than 3.3 eV are absorbed in the emitter layer, and photons in the range of 1-3.3 eV are absorbed in the CZTSe layer. High-energy photons that are absorbed in the CZTSe layer generate high-energy electrons. High-energy electrons are unstable, thermolyze and recombine very quickly. Therefore, when the band gap of the emitter layer decreased from 3.3 eV to 3 eV, the total output power increased. Because in MoO_3, photons between 3 eV and 3.3 eV generate stable electrons when absorbed and they participate in forming of current. Figure 4 shows the dependence of the short circuit current of n-ZnO/p-CZTSe/p-NiOx, n-TiO_2/p-CZTSe/p-NiO_x and n-MoO_3/p-CZTSe/p-NiO_x solar cells on emitter and base thickness. The short-circuit current density of n-ZnO/p-CZTSe/p-NiO_x varied depending on the emitter and base thickness similar to the output power. But this solar cell reached the maximum short-circuit current value of 30.72 mA/cm^2 with an emitter layer thickness of 80 nm and a base thickness of 5 μm. As the base thickness increased, the short-circuit current of n-TiO_2/p-CZTSe/p-NiO_x and n-MoO_3/p-CZTSe/p-NiO_x increased monotonically, unlike the output power.

When their base thickness is 5 μm and emitter layer thickness is 60 nm, the short-circuit current reached a maximum of 26.85 mA/cm^2 and 29.3 mA/cm^2. The short circuit of all three solar cells increased monotonically as the base thickness increased. Because when the thickness of the base increases, the concentration of electron-hole pairs generated in the base increases. But the short-circuit current also reached its maximum value at the optimal values of the emitter layer.

D. OPEN CIRCUIT VOLTAGE

As the thickness of the base increases, the open circuit voltage decreases. Figure 5 shows the open circuit voltage of n-ZnO/p-CZTSe/p-NiO_x, n-TiO_2/p-CZTSe/p-NiO_x and n-MoO_3/p-CZTSe/p-NiO_x solar cells as a function of base and emitter layer thickness. n-ZnO/p-CZTSe/p-NiO_x, n-TiO_2/p-CZTSe/p-NiO_x and n-MoO_3/p-CZTSe/p-NiO_x solar cells reached to maximum values of open circuit voltage of 0.66 V, 0.678 V and 0.69 V when base and emitter layer thicknesses are equal to 0.5 μm and 200 nm. The open

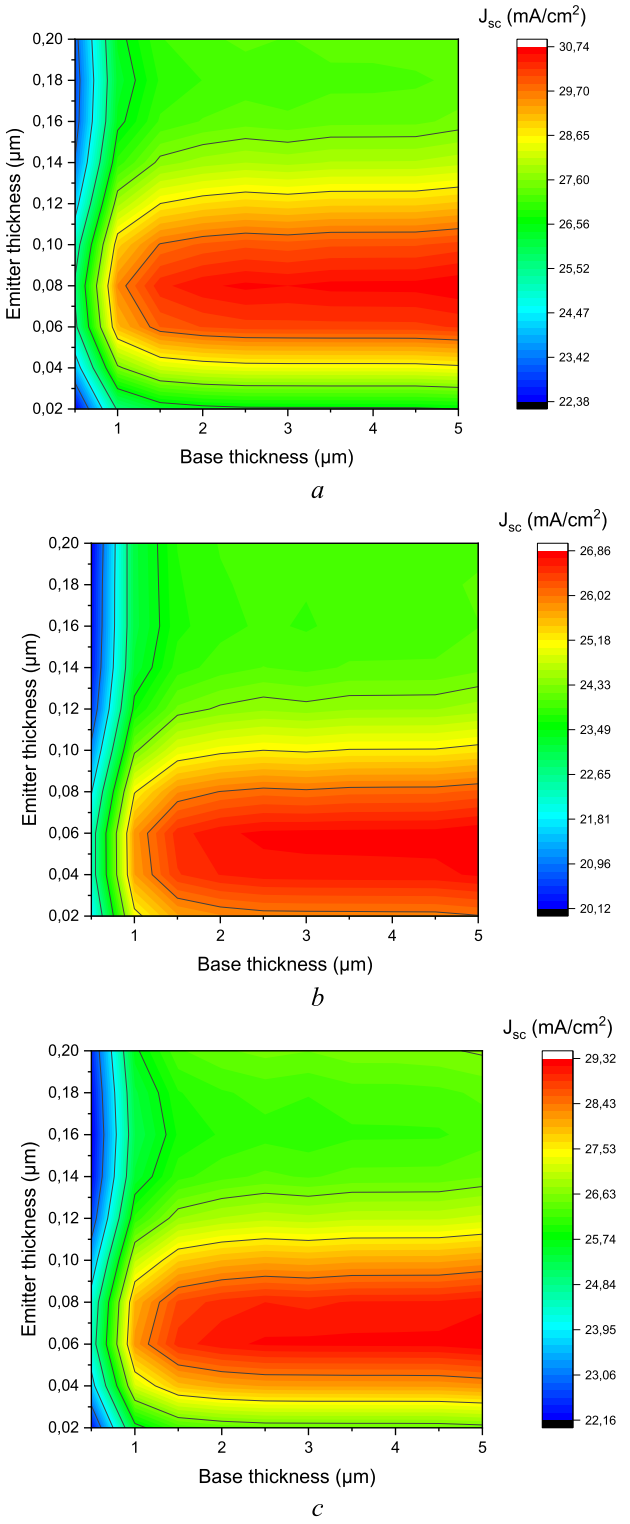

FIGURE 4. Dependence of short circuit current of n-ZnO/p-CZTSe/p-NiO_x (a), n-TiO_2/p-CZTSe/p-NiO_x (b) va n-MoO_3/p-CZTSe/p-NiO_x (c) on emitter layer and base thickness.

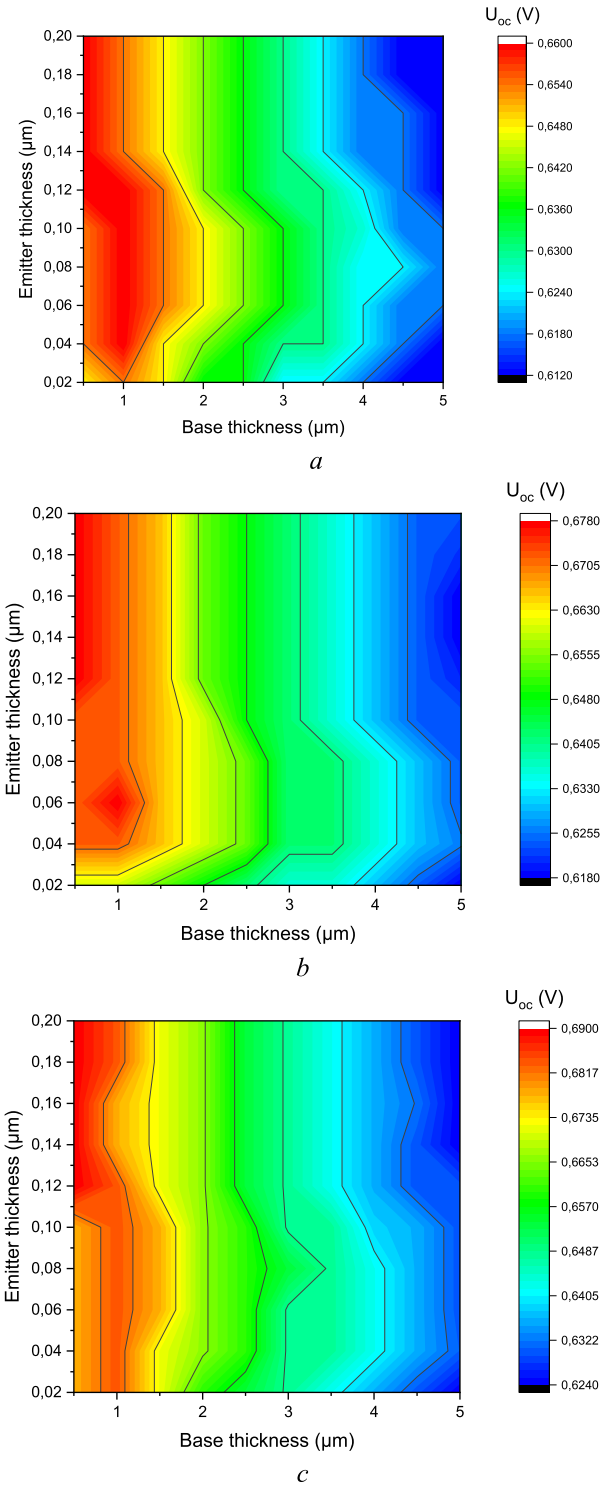

FIGURE 5. Dependence of open circuit voltage of n-ZnO/p-CZTSe/p-NiO_x (a), n-TiO_2/p-CZTSe/p-NiO_x (b) va n-MoO_3/p-CZTSe/p-NiO_x (c) solar cells on emitter layer and base thickness.

circuit voltage of each solar cell decreased as the CZTSe layer thickness increased. Because the series resistance can increase when the thickness of the base increases which causes the limitation of the voltage [45].

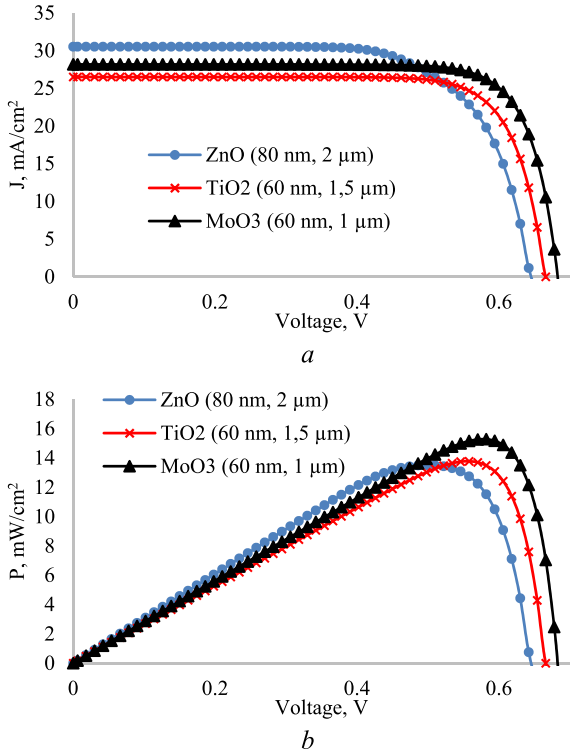

FIGURE 6. I-V (a) and P-V (b) characteristics of n-ZnO/p-CZTSe/p-NiO_x, n-TiO_2/p-CZTSe/p-NiO_x and n-MoO_3/p-CZTSe/p-NiO_x solar cells with emitter thickness of 80 nm, 60 nm, 60 nm and base thickness of 2 μm, 1.5 μm, 1 μm.

When the thickness of the emitter layer increased, the open circuit voltage also increased. The monotonous decrease of the open circuit voltage and the monotonous increase of the short-circuit current when the thickness of the base increases explain the fact that the function of the dependence of the output power on the thickness of the base can have an extremum.

Figure 6 shows the I-V and P-V charcateristics of n-ZnO/p-CZTSe/p-NiO_x, n-TiO_2/p-CZTSe/p-NiO_x, and n-MoO_3/p-CZTSe/p-NiO_x solar cells with optimal sizes. n-MoO_3/p-CZTSe/p-NiO_x with optimal size has higher output power and open circuit voltage than that of n-ZnO/p-CZTSe/p-NiOx by 1.69 mW/cm^2 and 0.03 V, but the short-circuit current density is smaller by 1.42 mA/cm^2.

E. FILL FACTOR

Since the open circuit voltage is almost the same, the short-circuit current of a solar cell with a high output power must also be high. But we observed the opposite in these solar cells. The steepness of the I-V characteristic of n-MoO_3/p-CZTSe/p-NiO_x compared to that of n-ZnO/p-CZTSe/p-NiO_x proves that its output power is higher. On the other hand, the high power can be explained by the fill factor. Figure 7 shows the fill factor of n-ZnO/p-CZTSe/p-NiO_x, n-TiO_2/p-CZTSe/p-NiO_x and n-MoO_3/p-CZTSe/p-NiO_x solar cells as a function of emitter and base layer thickness. The fill factor of the n-ZnO/p-CZTSe/p-NiO_x (Figure 7.a) solar cell increased as the base thickness increased. The fill factor

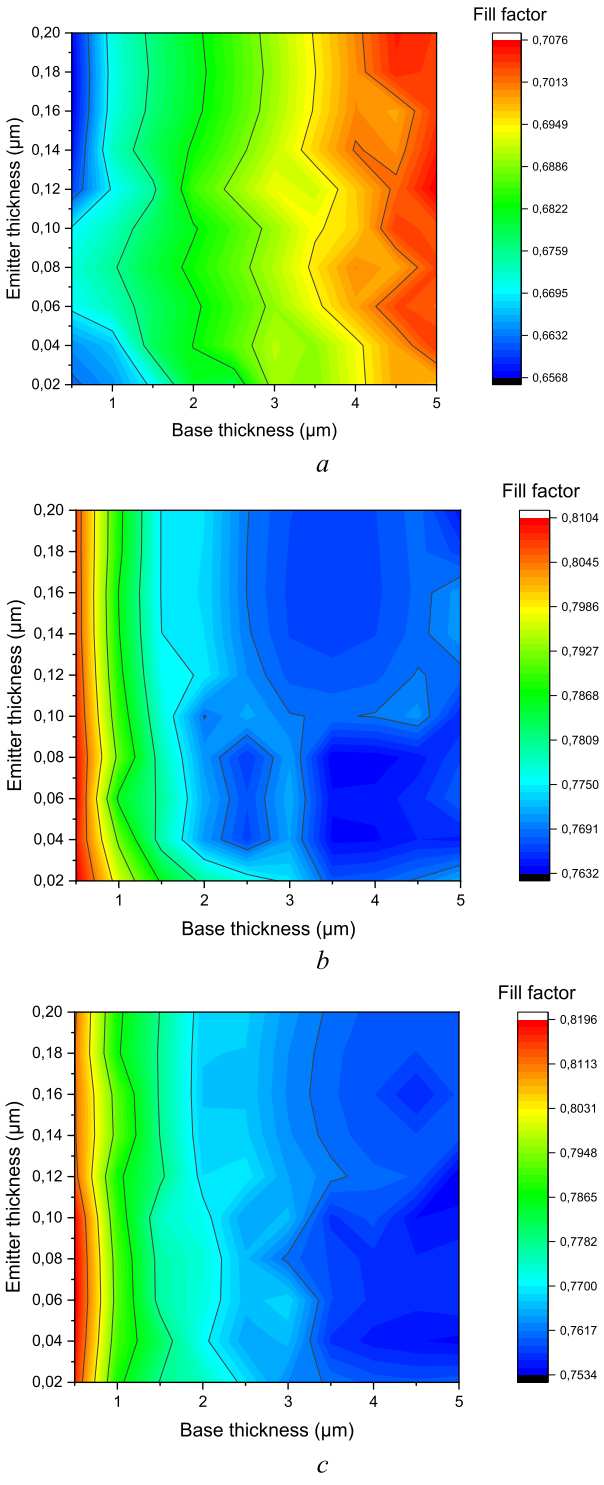

FIGURE 7. Dependence of gill factor of n-ZnO/p-CZTSe/p-NiO_x (a), n-TiO_2/p-CZTSe/p-NiO_x (b) and n-MoO_3/p-CZTSe/p-NiO_x (c) solar cells on emitter layer and base thickness.

of n-TiO_2/p-CZTSe/p-NiO_x (Figure 7.b) and n-MoO_3/p-CZTSe/p-NiO_x (Figure 7.c) solar cells decreased when the base thickness increased.

Naturally, when the thickness of the base of the solar cell increases, the series resistance increases, which causes the fill factor to decrease. The n-ZnO/p-CZTSe/p-NiO_x solar cell achieved a maximum fill factor of 0.7075 when the emitter and base layer thicknesses were 120 nm and 5 μm. n-TiO_2/p-CZTSe/p-NiO_x and n-MoO_3/p-CZTSe/p-NiO_x solar cells reached the maximum fill factor of 0.81 and 0.82 when the base and emitter layer thicknesses were 0.5 μm and 60 nm.

Due to the higher fill factor of n-MoO_3/p-CZTSe/p-NiO_x than n-ZnO/p-CZTSe/p-NiO_x, the maximum output power was also higher. The fill factor mainly indicates the quality of the surface, so the quality of passivation of the surface between the base and the emitter layer. The ITO/ZnO/CdS/CZTSe structure simulated in Silvaco TCAD showed a short-circuit current of 44 mA/cm^2, an open circuit voltage of 0.45 V, an efficiency of 12.2%, and a fill factor of 62.7% [46]. Since metal oxide is used as an emitter layer, it can simultaneously act as an anti-reflection and passivation layer [47].

F. OPTICAL PROPERTIES

To determine its anti-reflective properties, it is necessary to calculate its optical properties. Figure 8 shows the dependence of absorption, reflection and transmission coefficients solar cells with optimal sizes on light wavelength. It was found that the absorption coefficient of the n-ZnO/p-CZTSe/p-NiO_x solar cell is higher than that of other solar cells in visible region, and the reflection coefficient is lower.The higher absorption coefficient observed in the visible region for the n-ZnO/p-CZTSe/p-NiO_x solar cell can be attributed to the increased thickness of the base, influencing both optical and electrical properties. Leveraging ZnO as an emitter layer not only enhances absorption but also acts as an effective anti-reflection and passivation layer, contributing to its superior performance in CZTSe-based solar cells. The n-TiO_2/p-CZTSe/p-NiO_x solar cell was found to have the lowest absorption coefficient and the highest reflection coefficient. The higher absorption coefficient of n-ZnO/p-CZTSe/p-NiO_x can be justified by the thickness of the base. Moreover, the absorption and reflection coefficient showed that ZnO also acts as a better anti-reflection layer in the CZTSe-based solar cell.

In Figure 9, the dependence of the complex refractive index of ZnO [48], TiO_2 [49], MoO_3 [50], CZTSe [51] and NiO_x [52] on the wavelength is described. Air has a refractive index of 1 and CZTSe has an average refractive index of 2.85, the ideal antireflective coating should have a refractive index of 1.69 to minimize the CZTSe reflection coefficient.

The average refractive index of ZnO and MoO_3 (Figure 9.a) is 1.82 and 2.13. This proves that ZnO is the optimal optical material to use as optical coating for CZTSe. NiO_x has an average refractive index of 1.62, which is very close to the optimal value, but its electrical properties do not allow it to be used as an emitter. However, in further scientific research, the inverted CZTSe structure can be investigated. The abstract part of the complex refractive index shows the

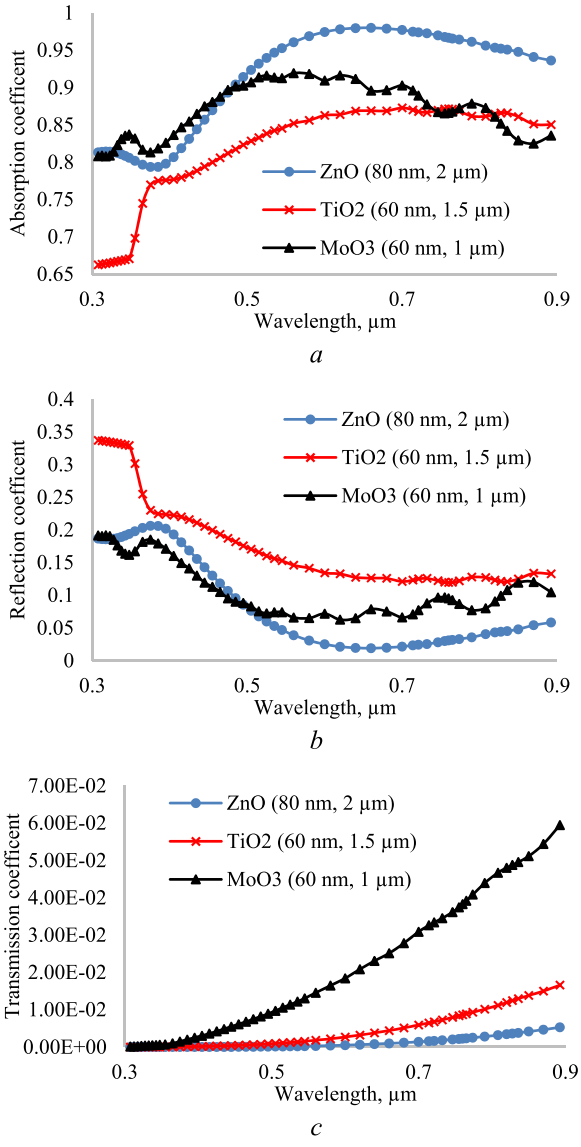

FIGURE 8. Dependence of absorption (a), reflection (b) and transmission coefficient (c) of n-ZnO/p-CZTSe/p-NiO_x, n-TiO_2/p-CZTSe/p-NiO_x and n-MoO_3/p-CZTSe/p-NiO_x solar cells with emitter thickness of 80 nm, 60 nm, 60 nm and base thickness of 2 μm, 1.5 μm, 1 μm.

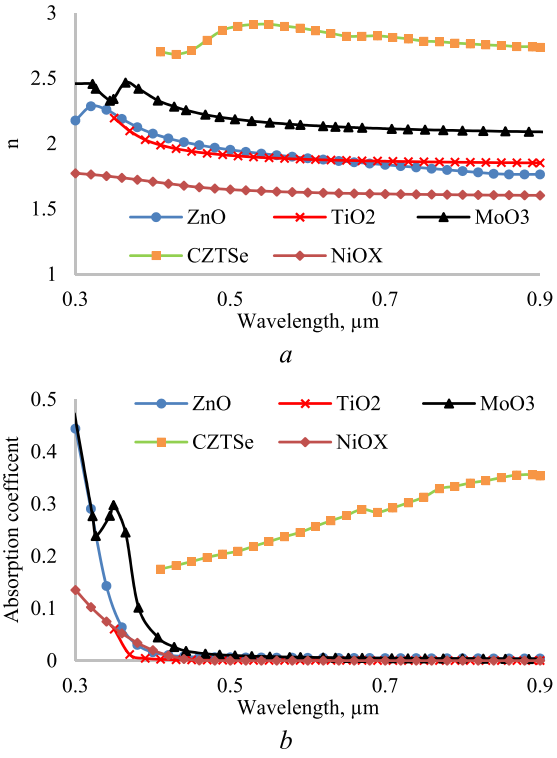

FIGURE 9. Real (a) and imaginary (b) part of complex refractive index of ZnO, TiO_2, MoO_3, CZTSe and NiO_x.

light absorption coefficient of the material. The abstract part of the complex refractive index of MoO_3 (Figure 9.b) is better than other metal oxides. Therefore, when the CZTSe surface is covered with MoO_3, the concentration of absorbed photons in the emitter layer is higher. Since there is more recombination in the emitter layer, not all photogenerated electrons can participate in carrier transport.

G. INTERNAL ELECTRIC FIELD

As the thickness of the base decreases, the transmission coefficient of the solar cells (Figure 8.c) increased. Because most of the photons are absorbed in the base. Therefore, the transmission coefficient of n-MoO_3/p-CZTSe/p-NiO_x was the highest. The short-circuit current of n-ZnO/p-CZTSe/p-NiO_x with optimal size was found to be higher compared to other solar cells. This is due to its high absorption coefficient. Therefore, the n-ZnO/p-CZTSe/p-NiO_x structure is an optically optimal system but not optimal as a solar cell. Its maximum power point current and voltage values are lower than those of other solar cells. Because it is also important that the photogenerated electron-holes reach the contacts in the solar cell. The magnitude of the fill factor indicates the smallness of the series resistance. Therefore, the series resistance of n-MoO_3/p-CZTSe/p-NiO_x structure is smaller than other structures. This proves its good transport properties. Because, according to our previous studies, the electron mobility in MoO_3 is 3811 $cm^2V^{-1}s^{-1}$ and in ZnO it is equal to 50 $cm^2V^{-1}s^{-1}$. If the mobility of electrons is high, there is a high probability that electrons from this layer will reach the electrodes without recombination. This proves that n-MoO_3/p-CZTSe/p-NiO_x solar cell has higher output power and fill factor than other structures. Figure 10 shows the distribution of electric field and electrostatic potential of n-ZnO/p-CZTSe/p-NiO_x, n-TiO_2/p-CZTSe/p-NiO_x, and n-MoO_3/p-CZTSe/p-NiO_x solar cells with equal thickness along with Y axis. The internal electric field at the p-n junction helps the photogenerated electron-hole pairs to separate and reach the contacts. The maximum values of internal electric field in n-ZnO/p-CZTSe/p-NiO_x, n-TiO_2/p-CZTSe/p-NiO_x and n-MoO_3/p-CZTSe/p-NiO_x solar cells (Figure 10.a) are equal to 3e4 V/cm, 8e4 V/cm and 1e6 V/cm, respectively. MoO_3 has a larger electrostatic potential

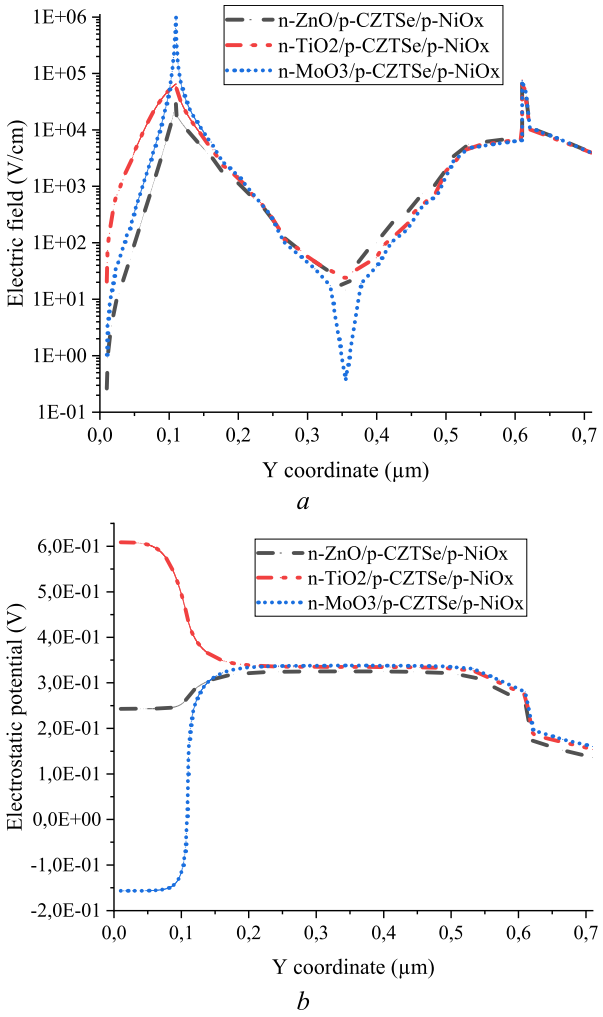

FIGURE 10. Distribution of electric field (a) and electrostatic potential (b) of n-ZnO/p-CZTSe/p-NiOx, n-TiO2/p-CZTSe/p-NiOx and n-MoO3/p-CZTSe/p-NiOx with emitter thickness of 100 nm and base thickness of 0.5 μm.

difference with CZTSe than other metal oxides, and it produced the largest electric field. Therefore, there is a high probability separation of electron-hole pairs formed at the base of the n-MoO_3/p-CZTSe/p-NiO_x solar cell and reaching to the contact. Therefore, its output power is greater than that of other solar cells. The n-ZnO/p-CZTSe/p-NiO_x structure with optimal sizes has a high absorption coefficient, but not all photogenerated electrons and holes can reach the contacts. Because its base is thick, which causes the amount of recombination in it to increase and the electric field in the base to decrease. Because the electric field strength in n-TiO_2/p-CZTSe/p-NiO_x solar cell and the electrostatic potential difference between n-TiO_2/p-CZTSe layers are larger than in n-ZnO/p-CZTSe/p-NiO_x, it has also higher output power.

IV. CONCLUSION

In summary, this study explored CZTSe-based solar cells by investigating the impact of different charge transport layers. Using ZnO, TiO_2, MoO_3 as electron transport layers (ETL), and NiO_x as the hole transport layer (HTL), we found that choosing the right materials enhances charge carrier separation and reduces surface recombination. Our analysis, which included band diagrams, electronic affinities, and band offsets, confirmed the suitability of ZnO, TiO_2, MoO_3, and NiO_x for their respective roles. Optimal layer thicknesses were crucial for achieving maximum solar cell efficiency and increased power output. Notably, the n-MoO_3/p-CZTSe/p-NiO_x design stood out with its excellent electron transport characteristics, evident in its steep I-V curve and high fill factor. ZnO played a vital role as an effective anti-reflective coating, enhancing light absorption in the CZTSe layer. The interaction between light absorption, carrier extraction, and layer dimensions affected short-circuit current and open-circuit voltage under varying conditions. MoO_3's elevated electron mobility significantly boosted the performance of the n-MoO_3/p-CZTSe/p-NiO_x solar cell by ensuring efficient carrier transport to the contacts. Our findings not only advance the understanding of CZTSe-based solar cells but also provide valuable insights into the nuanced interrelationships among charge transport layers, layer thicknesses, and material properties. This comprehensive exploration lays a foundation for the continued optimization of CZTSe solar cells and opens avenues for the development of sustainable and high-performance photovoltaic technologies. Future research could explore inverted structures and advanced passivation strategies to further improve the efficiency of these innovative solar cell configurations. Future experimental studies hold the potential to refine and validate these results, contributing to a deeper understanding and continuous enhancement of the performance of CZTSe-based solar cells.

REFERENCES

[1] D. Lee, A. Lee, and H.-D. Kim, "IZO/ITO double-layered transparent conductive oxide for silicon heterojunction solar cells," *IEEE Access*, vol. 10, pp. 77170–77175, 2022, doi: 10.1109/ACCESS.2022.3192646.

[2] W. Shockley and H. J. Queisser, "Detailed balance limit of efficiency of *p-n* junction solar cells," *J. Appl. Phys.*, vol. 32, no. 3, pp. 510–519, Mar. 1961, doi: 10.1063/1.1736034.

[3] J. Kim, S. Lee, S. Park, M. Ju, Y. Kim, E.-C. Cho, S. K. Dhungel, and J. Yi, "Highly efficient bifacial silicon/silicon tandem solar cells," *IEEE Access*, vol. 11, pp. 21326–21331, 2023, doi: 10.1109/ACCESS.2023.3248795.

[4] J. Gulomov and O. Accouche, "Gold nanoparticles introduced ZnO/perovskite/silicon heterojunction solar cell," *IEEE Access*, vol. 10, pp. 119558–119565, 2022, doi: 10.1109/ACCESS.2022.3221875.

[5] A. H. Sabeeh, A. N. Brigeman, and J. Ruzyllo, "Performance of single-crystal silicon solar cells with mist-deposited nanocrystalline quantum dot downshifting films," *IEEE J. Photovolt.*, vol. 9, no. 4, pp. 1006–1011, Jul. 2019, doi: 10.1109/JPHOTOV.2019.2914439.

[6] J. Gulomov and R. Aliev, "The way of the increasing two times the efficiency of silicon solar cell," *Phys. Chem. Solid State*, vol. 22, no. 4, pp. 756–760, Dec. 2021, doi: 10.15330/PCSS.22.4.756-760.

[7] K. Chakraborty, M. G. Choudhury, and S. Paul, "Study of physical, optical, and electrical properties of cesium titanium (IV)-based single halide perovskite solar cell," *IEEE J. Photovolt.*, vol. 11, no. 2, pp. 386–390, Mar. 2021, doi: 10.1109/JPHOTOV.2021.3050268.

[8] S. Jirage, P. Pagare, K. Garadkar, S. Delekar, and V. Bhuse, "Novel chemical approach to synthesis and characterization of greener and rock-like Cu_2ZnSnS_3Se (CZTSSe) thin films of Kasterite structure," *Mater. Today, Proc.*, vol. 43, pp. 2774–2779, Jan. 2021, doi: 10.1016/J.MATPR.2020.07.704.

[9] S. A. Moiz, A. N. M. Alahmadi, and A. J. Aljohani, "Design of a novel lead-free perovskite solar cell for 17.83% efficiency," *IEEE Access*, vol. 9, pp. 54254–54263, 2021, doi: 10.1109/ACCESS.2021.3070112.

[10] H. Katagiri, K. Jimbo, W. S. Maw, K. Oishi, M. Yamazaki, H. Araki, and A. Takeuchi, "Development of CZTS-based thin film solar cells," *Thin Solid Films*, vol. 517, no. 7, pp. 2455–2460, Feb. 2009, doi: 10.1016/J.TSF.2008.11.002.

[11] L. Grenet, F. Emieux, L. Choubrac, J. A. Márquez, E. De Vito, F. Roux, and T. Unold, "Surface preparation for 10% efficient CZTSe solar cells," *Prog. Photovoltaics, Res. Appl.*, vol. 29, no. 2, pp. 188–199, Feb. 2021, doi: 10.1002/PIP.3356.

[12] D. Zhang, S. Sun, X. Li, X. Li, X. Liu, Q. Li, H. Liao, and S. Wang, "Preparing $Cu_2ZnSn(S_xSe_{1-x})_4$ thin-film solar cells with front band gap grading by plasma sulfurization," *Sol. Energy*, vol. 227, pp. 516–524, Oct. 2021, doi: 10.1016/J.SOLENER.2021.08.073.

[13] Z. Zhang, Q. Gao, J. Guo, Y. Zhang, Y. Han, J. Ao, M.-J. Jeng, F. Liu, W. Liu, and Y. Zhang, "Over 10% efficient pure CZTSe solar cell fabricated by electrodeposition with Ge doping," *Sol. RRL*, vol. 4, no. 5, May 2020, Art. no. 2000059, doi: 10.1002/SOLR.202000059.

[14] U. Saha, A. Biswas, and M. K. Alam, "Efficiency enhancement of CZTSe solar cell using CdS(n)/$(Ag_xCu_{1-x})_2ZnSnSe_4$ (p) /$Cu_2ZnSnSe_4$ (p+) structure," *Sol. Energy*, vol. 221, pp. 314–322, Jun. 2021, doi: 10.1016/J.SOLENER.2021.04.043.

[15] D. Talukder, R. Pal, M. N. Hasan, and Md. F. Wahid, "Numerical simulation of CZTS solar cell with ZnSe buffer layer," in *Proc. Int. Conf. Autom., Control Mechatronics Ind. 4.0 (ACMI)*, Jul. 2021, pp. 1–6, doi: 10.1109/ACMI53878.2021.9528287.

[16] M. Minbashi, A. Ghobadi, E. Yazdani, A. A. Kordbacheh, and A. Hajjiah, "Efficiency enhancement of CZTSSe solar cells via screening the absorber layer by examining of different possible defects," *Sci. Rep.*, vol. 10, no. 1, pp. 1–14, Dec. 2020, doi: 10.1038/s41598-020-75686-2.

[17] W. C. Zhang, J. Y. Tang, Y. H. Niu, R. Huang, L. Chen, and M. Y. Jiang, "Study the best ratio of S and Se in CZTSSe solar cells with nontoxic buffer layer," *J. Renew. Sustain. Energy*, vol. 13, no. 3, May 2021, Art. no. 033701, doi: 10.1063/5.0046648/285093.

[18] S. Amiri and S. Dehghani, "Design of highly efficient CZTS/CZTSe tandem solar cells," *J. Electron. Mater.*, vol. 49, no. 3, pp. 2164–2172, Mar. 2020, doi: 10.1007/s11664-019-07898-w.

[19] Z. Seboui and S. Dabbabi, "First investigation on CZTS electron affinity and thickness optimization using SILVACO-atlas 2D simulation," *Simul. Model. Pract. Theory*, vol. 126, Jul. 2023, Art. no. 102758, doi: 10.1016/J.SIMPAT.2023.102758.

[20] K.-H. Lee, K. Araki, and M. Yamaguchi, "A mesh downsampling algorithm for equivalent circuit network simulation of multi-junction solar cells," *IEEE Access*, vol. 7, pp. 97208–97215, 2019, doi: 10.1109/ACCESS.2019.2930002.

[21] U. Saha and M. K. Alam, "Proposition and computational analysis of a kesterite/kesterite tandem solar cell with enhanced efficiency," *RSC Adv.*, vol. 7, no. 8, pp. 4806–4814, Jan. 2017, doi: 10.1039/C6RA25704F.

[22] S. Ahn, S. Jung, J. Gwak, A. Cho, K. Shin, K. Yoon, and J. H. Yun, "Band gap determination of $Cu_2ZnSnSe_4$ thin films," in *Proc. 35th IEEE Photovoltaic Specialists Conf.*, Jun. 2010, pp. 1894–1896, doi: 10.1109/PVSC.2010.5616301.

[23] L. Et-taya, A. Benami, and T. Ouslimane, "Study of CZTSSe-based solar cells with different ETMs by SCAPS," *Sustainability*, vol. 14, no. 3, p. 1916, Feb. 2022, doi: 10.3390/SU14031916.

[24] G. A. Casas, M. A. Cappelletti, A. P. Cédola, B. M. Soucase, and E. L. P. Y. Blancá, "Analysis of the power conversion efficiency of perovskite solar cells with different materials as hole-transport layer by numerical simulations," *Superlattices Microstructures*, vol. 107, pp. 136–143, Jul. 2017, doi: 10.1016/J.SPMI.2017.04.007.

[25] J. Gulomov, O. Accouche, R. Aliev, R. Ghandour, and I. Gulomova, "Investigation of n-ZnO/p-Si and n-TiO_2/p-Si heterojunction solar cells: TCAD+DFT," *IEEE Access*, vol. 11, pp. 38970–38981, 2023, doi: 10.1109/ACCESS.2023.3268033.

[26] D. P. Norton, Y. W. Heo, M. P. Ivill, K. Ip, S. J. Pearton, M. F. Chisholm, and T. Steiner, "ZnO: Growth, doping & processing," *Mater. Today*, vol. 7, no. 6, pp. 34–40, Jun. 2004, doi: 10.1016/S1369-7021(04)00287-1.

[27] K. Davis, R. Yarbrough, M. Froeschle, J. White, and H. Rathnayake, "Band gap engineered zinc oxide nanostructures via a sol–gel synthesis of solvent driven shape-controlled crystal growth," *RSC Adv.*, vol. 9, no. 26, pp. 14638–14648, May 2019, doi: 10.1039/C9RA02091H.

[28] K. B. Sundaram and A. Khan, "Work function determination of zinc oxide films," *J. Vac. Sci. Technol. A, Vac., Surf., Films*, vol. 15, no. 2, pp. 428–430, Mar. 1997, doi: 10.1116/1.580502.

[29] J. Gulomov, O. Accouche, Z. Al Barakeh, R. Aliev, I. Gulomova, and B. Neji, "Atom-to-device simulation of MoO_3/Si heterojunction solar cell," *Nanomaterials*, vol. 12, no. 23, p. 4240, Nov. 2022, doi: 10.3390/NANO12234240.

[30] M. Shahrokhi, P. Raybaud, and T. Le Bahers, "On the understanding of the optoelectronic properties of S-doped MoO_3 and O-doped MoS_2 bulk systems: A DFT perspective," *J. Mater. Chem. C*, vol. 8, no. 26, pp. 9064–9074, Jul. 2020, doi: 10.1039/D0TC02066D.

[31] S. Wahid, M. Islam, M. S. S. Rahman, and M. K. Alam, "Transfer matrix formalism-based analytical modeling and performance evaluation of perovskite solar cells," *IEEE Trans. Electron Devices*, vol. 64, no. 12, pp. 5034–5041, Dec. 2017, doi: 10.1109/TED.2017.2763091.

[32] K. Jäger, R. A. C. M. M. van Swaaij, and M. Zeman, "The scalar scattering theory: A multi-functional tool for optimizing scattering in thin-film silicon solar cells," in *Proc. Renew. Energy Environ. Opt. Photon. Congr.*, Nov. 2012, Paper no. PT3C.7, doi: 10.1364/PV.2012.PT3C.7.

[33] J. Escarré, F. Villar, J. M. Asensi, J. Bertomeu, and J. Andreu, "Spectral analysis of the angular distribution function of back reflectors for thin film silicon solar cells," *J. Non-Crystalline Solids*, vol. 352, nos. 9–20, pp. 1896–1899, Jun. 2006, doi: 10.1016/J.JNONCRYSOL.2005.12.046.

[34] G. Lérondel and R. Romestain, "Fresnel coefficients of a rough interface," *Appl. Phys. Lett.*, vol. 74, no. 19, pp. 2740–2742, May 1999, doi: 10.1063/1.123999.

[35] L. Chen and H. Bagci, "Steady-state simulation of semiconductor devices using discontinuous Galerkin methods," *IEEE Access*, vol. 8, pp. 16203–16215, 2020, doi: 10.1109/ACCESS.2020.2967125.

[36] S. Kola, J. M. Golio, and G. N. Maracas, "An analytical expression for Fermi level versus sheet carrier concentration for HEMT modeling," *IEEE Electron Device Lett.*, vol. EDL-9, no. 3, pp. 136–138, Mar. 1988, doi: 10.1109/55.2067.

[37] A. S. Lin and J. D. Phillips, "Drift-diffusion modeling for impurity photovoltaic devices," *IEEE Trans. Electron Devices*, vol. 56, no. 12, pp. 3168–3174, Dec. 2009, doi: 10.1109/TED.2009.2032741.

[38] N. Kamarulzaman, M. F. Kasim, and R. Rusdi, "Band gap narrowing and widening of ZnO nanostructures and doped materials," *Nanosci. Res. Lett.*, vol. 10, no. 1, pp. 1–12, Dec. 2015, doi: 10.1186/S11671-015-1034-9.

[39] J. Zhang, P. Zhou, J. Liu, and J. Yu, "New understanding of the difference of photocatalytic activity among anatase, rutile and brookite TiO_2," *Phys. Chem. Chem. Phys.*, vol. 16, no. 38, pp. 20382–20386, Sep. 2014, doi: 10.1039/C4CP02201G.

[40] A. K. M. Hasan, K. Sobayel, I. Raifuku, Y. Ishikawa, M. Shahiduzzaman, M. Nour, H. Sindi, H. Moria, M. Rawa, K. Sopian, N. Amin, and M. Akhtaruzzaman, "Optoelectronic properties of electron beam-deposited NiOx thin films for solar cell application," *Results Phys.*, vol. 17, Jun. 2020, Art. no. 103122, doi: 10.1016/J.RINP.2020.103122.

[41] S. Santhosh, M. Mathankumar, S. S. Chandrasekaran, A. K. N. Kumar, P. Murugan, and B. Subramanian, "Effect of ablation rate on the microstructure and electrochromic properties of pulsed-laser-deposited molybdenum oxide thin films," *Langmuir*, vol. 33, no. 1, pp. 19–33, Jan. 2017, doi: 10.1021/acs.langmuir.6b02940.

[42] S. Sharbati and J. R. Sites, "Impact of the band offset for n-Zn(O, S)/p-Cu(In, Ga)Se_2 solar cells," *IEEE J. Photovolt.*, vol. 4, no. 2, pp. 697–702, Mar. 2014, doi: 10.1109/JPHOTOV.2014.2298093.

[43] Q. Sun, J. Tang, C. Zhang, Y. Li, W. Xie, H. Deng, Q. Zheng, J. Wu, and S. Cheng, "Efficient environmentally friendly flexible CZTSSe/ZnO solar cells by optimizing ZnO buffer layers," *Materials*, vol. 16, no. 7, p. 2869, Apr. 2023, doi: 10.3390/MA16072869/S1.

[44] S. Ranjbar, G. Brammertz, B. Vermang, A. Hadipour, S. Cong, K. Suganuma, T. Schnabel, M. Meuris, A. F. da Cunha, and J. Poortmans, "Improvement of kesterite solar cell performance by solution synthesized MoO_3 interfacial layer," *Phys. Status Solidi A*, vol. 214, no. 1, Jan. 2017, Art. no. 1600534, doi: 10.1002/PSSA.201600534.

[45] X. Hu, Y. Wang, Y. Jia, J. Hong, T. Chen, J. Xue, Y. Chen, J. Tao, G. Weng, S. Chen, Z. Zhu, and J. Chu, "Resistive effects on the spatially resolved absolute electroluminescence of thin-film Cu(In, Ga)Se_2 solar cells studied by a distributed two-diode model," *IEEE Access*, vol. 8, pp. 112859–112866, 2020, doi: 10.1109/ACCESS.2020.3002659.

[46] T. J. Mebelson and K. Elampari, "A study of electrical and optical characteristics of CZTSe solar cell using Silvaco Atlas," *Mater. Today, Proc.*, vol. 46, pp. 2540–2543, Jan. 2021, doi: 10.1016/J.MATPR.2021.01.758.

[47] D. Wang, Y. Wang, J. Huang, W. Fu, Y. Lei, P. Deng, H. Cai, and J. Liu, "Low-cost and flexible anti-reflection films constructed from nano multi-layers of TiO_2 and SiO_2 for perovskite solar cells," *IEEE Access*, vol. 7, pp. 176394–176403, 2019, doi: 10.1109/ACCESS.2019.2957583.
[48] L. Fanni, B. Delaup, B. Niesen, Y. Milstein, D. Shachal, M. Morales-Masis, S. Nicolay, and C. Ballif, "Tuning the porosity of zinc oxide electrodes: From dense to nanopillar films," *Mater. Res. Exp.*, vol. 2, no. 7, Jul. 2015, Art. no. 075006, doi: 10.1088/2053-1591/2/7/075006.
[49] J. Cui, T. Allen, Y. Wan, J. Mckeon, C. Samundsett, D. Yan, X. Zhang, Y. Cui, Y. Chen, P. Verlinden, and A. Cuevas, "Titanium oxide: A re-emerging optical and passivating material for silicon solar cells," *Sol. Energy Mater. Sol. Cells*, vol. 158, pp. 115–121, Dec. 2016, doi: 10.1016/J.SOLMAT.2016.05.006.
[50] L. Lajaunie, F. Boucher, R. Dessapt, and P. Moreau, "Strong anisotropic influence of local-field effects on the dielectric response of α-MoO_3," *Phys. Rev. B, Condens. Matter*, vol. 88, no. 11, Sep. 2013, Art. no. 115141, doi: 10.1103/PhysRevB.88.115141.
[51] H. ElAnzeery, O. El Daif, M. Buffière, S. Oueslati, K. B. Messaoud, D. Agten, G. Brammertz, R. Guindi, B. Kniknie, M. Meuris, and J. Poortmans, "Refractive index extraction and thickness optimization of $Cu_2ZnSnSe_4$ thin film solar cells," *Phys. Status Solidi A*, vol. 212, no. 9, pp. 1984–1990, Sep. 2015, doi: 10.1002/PSSA.201431807.
[52] S. Manzoor, J. Häusele, K. A. Bush, A. F. Palmstrom, J. Carpenter, Z. J. Yu, S. F. Bent, M. D. Mcgehee, and Z. C. Holman, "Optical modeling of wide-bandgap perovskite and perovskite/silicon tandem solar cells using complex refractive indices for arbitrary-bandgap perovskite absorbers," *Opt. Exp.*, vol. 26, no. 21, pp. 27441–27460, Oct. 2018, doi: 10.1364/OE.26.027441.

JASURBEK GULOMOV was born in Andijan, Uzbekistan, in 1999. He received the B.S. degree in physics and the M.S. degree in physics of renewable energy sources and sustainable environment from Andijan State University, Uzbekistan, in 2021 and 2023, respectively. He is the author of 21 articles and seven inventions. His research interests include numerical simulation, DFT, perovskites, nanoplasmonic solar cells, metal nanoparticles, metal oxides, heterojunction solar cells, computational material science, and programming. He is the Holder of a National Scholarship after being named Mirzo Ulugbek and the Winner of Student of the Year, in 2021. Besides, he is the Winner of President Scholarship, in 2022.

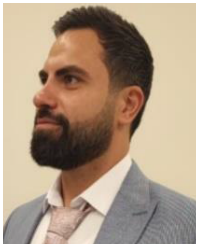

OUSSAMA ACCOUCHE (Member, IEEE) received the degree in electrical engineering from Lebanese University, Beirut, Lebanon, in 2011, and the master's and Ph.D. degrees in smart grids from Grenoble-Alpes University, Grenoble, France, in 2016. He has several years of industrial and international experience, including France, Italy, and Japan, as a supervisor engineer. Since September 2018, he has been an Assistant Professor with the Electrical Engineering Department, American University of the Middle East, Egaila, Kuwait. His research interests include smart grids, renewable energies, solar cells, artificial intelligence, and smart cities.

JAKHONGIR ZIYOITDINOV was born in Andijan, Uzbekistan, in 1988. He is currently the Secretary of the Scientific Council with Andijan State University and an Associate Professor with the Physics Department. Total teaching experience ten years. He has extensive experience in republic projects. He was involved in the following projects, such as "Improved solar energy usage." He participated in a seminar of such countries as Italy, Germany, and China. There are more than 70 scientific publications in international and local journals, conference proceedings, and periodicals. His research interests include numerical simulation, temperature effect on silicon, and cooling systems of PV panels.

AVAZBEK MIRZAALIMOV was born in Andijan, Uzbekistan. He is currently an Assistant Professor with the General Physics Department, Andijan State University. Total teaching experience ten years. He has graduated training course with Tianjin University. He participated in a seminar of such countries as Russia and China. There are more than 50 scientific publications in international and local journals, conference proceedings, and periodicals. His research interests include vertical junction solar cells, high voltage solar cells, and concentrators.